Formation of the hollow 1s0 1S state of Ne2+ by electron impact: Observation by means of an Auger hypersatellite

Article *in* Physical Review A · August 2000

DOI: 10.1103/PhysRevA.62.022704

CITATIONS
21

READS
210

7 authors, including:

Primož Pelicon
Jožef Stefan Institute
209 PUBLICATIONS **2,813** CITATIONS

SEE PROFILE

Iztok Čadež
Jožef Stefan Institute
95 PUBLICATIONS **1,264** CITATIONS

SEE PROFILE

Formation of the hollow $1s^o\,^1S$ state of Ne^{2+} by electron impact: Observation by means of an Auger hypersatellite

P. Pelicon,[1] I. Čadež,[1] M. Žitnik,[1] Ž. Šmit,[1,*] S. Dolenc,[1] A. Mühleisen,[1] and R. I. Hall[2]
[1]*J. Stefan Institute, P.O. Box 3000, SI-1001 Ljubljana, Slovenia*
[2]*DIAM, Université Pierre et Marie Curie, 4 place Jussieu, 75252 Paris 5, France*
(Received 18 October 1999; revised manuscript received 29 February 2000; published 13 July 2000)

A weak Auger transition at 870.5 ± 0.3 eV has been observed in neon for electron impact energies above the double *K*-shell ionization threshold (1863 eV). The Auger energies and transition rates identify the transition as the strongest Auger hypersatellite decay channel, $KK\text{-}KL_{23}L_{23}{}^2D$, of the hollow $1s^o\,^1S$ state of Ne^{2+}. The production cross section of the $1s^o\,^1S$ state by electron impact was determined for energies up to three times the threshold ionization energy and found to agree reasonably with the binary encounter calculations.

PACS number(s): 34.80.Dp, 31.15.Ne, 32.80.Hd, 34.50.Fa

I. INTRODUCTION

Since the observation of hollow atomic states formed by the scattering of highly charged ions from metal surfaces [1], these exotic atomic states with empty inner shells have become a subject of renewed interest. The identification of hollow states is usually made by observation of the x-ray or Auger decay channels. The decay channels of states with an empty *K* shell are known as hypersatellite transitions and have been intensively investigated in x-ray spectra excited by photons [2], electrons [3], and ions [4,5]. For double *K*-shell-vacancy states of light atoms, decay by Auger electron emission is more probable than photon emission. Thus, the cross sections for hollow state formation can be evaluated from measurements of Auger decay channels as the error introduced by the weak fluorescence yield is small [8]. Herein, we present a theoretical and experimental study of the formation of the $Ne^{2+}\,1s^o\,^1S$ state by electron impact, based on the detection of its $KK\text{-}KL_{23}L_{23}{}^2D$ hypersatellite Auger decay.

Krause *et al.* [6] recorded the Auger spectrum of neon at an electron impact energy of 4.5 keV and observed a transition at 870.3 eV. This feature was tentatively proposed to result from a satellite transition, but neither the initial nor final states were identified. Šmit *et al.* [7] made observations at 5 keV and the structure near 870 eV was interpreted as a $KK\text{-}KL_{23}L_{23}$ (^2S,^2P,^2D) triplet with comparable intensities. However, MCDF calculations of the Auger rates by Chen [8] and herein showed that the ^2D transition should be dominant, with ^2S reaching only about 20% of its intensity, while ^2P is negligible.

The hypersatellite transitions from the initial $1s^o\,^1S$ state may overlap with two groups of transitions: satellite transitions of the diagram $KL_{23}L_{23}$ transitions and hypersatellite transitions of states with a doubly ionized *K* shell and additionally excited or ionized *L*-shell electrons. The first ones, satellites of the diagram $KL_{23}L_{23}$ transitions, can be identified by measuring their excitation function. If they are observed in the spectra at the excitation energies below the threshold energy of the double *K*-shell ionization, then they are undoubtedly associated with the single *K*-shell ionization. The second group, the ''satellites'' of the hypersatellites, originate from the decay of initial states with a doubly ionized *K* shell and additionally excited or ionized *L*-shell electrons. To estimate their contribution to the measured spectra, we rely on the transition energy calculations and on the analogy with the satellites of the diagram *KLL* Auger lines.

For impact of 4.5 keV electrons, the intensity of the strongest satellite line of the diagram *KLL* Auger transitions, $1s^1 2p^5(^3P)\text{-}2p^3(^2D)$, does not exceed 0.06 of the strongest $KL_{23}L_{23}{}^1D_2$ diagram line. The strongest group of the satellite transitions originating from the configurations $1s^1 2p^5$ and $1s^1 2s^1 2p^6$ is spread over a 60 eV broad interval. The calculated shakeoff probability for the production of satellite states is 0.16 [7]. Total intensity of satellite lines is 0.21 of the total *KLL* Auger spectrum measured at 4.5 keV electron impact energy. Therefore, for the case of single *K*-shell electron impact ionization, shakeoff is responsible for most of the satellite state formations.

For the double *K*-shell ionization of neon, Šmit *et al.* [7] estimated the shakeoff probability of at least one $2p$ electron to be 0.46. Parallel to the electron-impact double *K*-shell ionization, the outer shell electrons may also be affected by multiple-encounter and multiple-step processes due to the interaction between the slow outgoing electrons and outer-shell electrons. The observation of hypersatellites in Na x-ray spectra [9] induced by electrons showed that the probability of creating a single $2p$ vacancy after removing two *K*-shell electrons is 0.33. The calculated shakeoff probability for this case is 0.36 and 0.28 for hydrogen and Hartree-Fock wave functions, respectively [7]. This shows that the shakeoff accounts for most of the probability that leads to the additionally excited or ionized *L* shell during the double *K*-shell ionization.

For the case of electron impact excitation, we therefore conclude that the total intensity of satellites of hypersatellites is comparable to the total intensity of the parent lines, but their individual intensities are well below the intensity of the strongest $KK\text{-}KL_{23}L_{23}{}^2D$ hypersatellite transition.

*Also at the Department of Physics, University of Ljubljana, Ljubljana, Slovenia.

TABLE I. Calculated transition energies, relative intensities, and natural widths of the Auger decay channels of the $Ne^{2+}\ 1s^{o}\ ^{1}S$ state. This work: MCDF, initial state frozen orbital approximation; Chen [8]: MCDF, final state frozen orbital approximation; Bhalla *et al.* [14]: Herman-Skillman wave functions.

Transition		Transition energy (eV) [11]	Relative intensity [%]			Natural width (eV)
			This work	Chen [8]	Bhalla [14]	
	^2D	872.2	49.2	44.0		
KK-$KL_{23}L_{23}$	^2P	871.3	0.3	0.4	66.2	0.819
	^2S	868.7	9.2	12.6		
	$^2P^{(-)}$	844.3	1.1	0.7	25.0	0.822
KK-KL_1L_{23}	$^2P^{(+)}$	837.1	33.0	31.6		
KK-KL_1L_1	^2S	812.9	7.0	10.7	7.9	0.852
		Total rate (a.u.)	$\Sigma = 22{,}9\times 10^{-3}$	$\Sigma = 29{,}6\times 10^{-3}$	$\Sigma = 26.0\times 10^{-3}$	

The electron impact double K-shell ionization cross section σ_{KK} can be scaled from the heavier already measured elements down to neon by means of a universal power law, $\sigma_{KK} \propto Z^{-6.63}$ [10]. Accordingly, σ_{KK} is expected to reach a maximum value of 30 ± 10 barn at between two and three times the threshold ionization energy.

II. CALCULATIONS

The decay energies, transition rates, and natural linewidths for the nonradiative channels of the $Ne^{2+}1s^{o}\ ^{1}S$ atomic state were calculated prior to the measurements.

To enable the calculations of nonradiative transition rates, the multiconfigurational Dirac-Fock code [11] was adopted to deal with the continuum wavefunctions [12]. Initial and final states were described by atomic wave functions using one-electron orbitals frozen in the initial state. From the relevant electron configurations $1s^1 2s^0$, $1s^1 2s^1 2p^5$, and $1s^1 2p^4$, 16 final states can be constructed in the j-j coupling limit. The atomic wave functions ($\mathcal{A}$) within the MCDF atomic model are presented as a linear combination in the basis set of configurational wave functions, eigenstates in the pure j-j coupling:

$$\mathcal{A}_\beta(\Gamma PJM) = \sum_\lambda c_{\beta\lambda}\mathcal{C}_\lambda(\gamma PJM). \tag{1}$$

The transition probability for nonradiative transition from the initial state $\mathcal{A}(J_i)$ into final state $\mathcal{A}(J_f)$ is then calculated as [13]

$$T_{i\to f} = 2\pi \sum_j \left| \sum_\lambda \sum_{\lambda'} c_{i\lambda} c_{f\lambda'} \left\langle \mathcal{C}_\lambda(J_i M_i) \right| \times \left| \sum_{\mu>\nu} r_{\mu\nu}^{-1} \right| \mathcal{C}_{\lambda'}(J_f M_f)\varepsilon l j; J_i M_i \right\rangle \right|^2. \tag{2}$$

The complete final state is constructed from the atomic final state $\mathcal{A}(J_f)$ and continuum electron state $|\varepsilon l j\rangle$. Presenting the final states $\mathcal{A}(J_f)$ in the basis set of 16 possible configuration states, the final-ionic-state configurational interaction (FISCI) was taken into account. In Table I, our transition rates are compared to those of Chen [8], obtained with the MCDF model in the final-state frozen-orbital approximation, and Bhalla [14], obtained with Herman-Skillman wave functions.

The transition energies were obtained from the difference between the total energies of the initial and final atomic states. Using the MCDF atomic model, typical deviations from the experimental transition energies are of order of 1 eV, when single inner-shell vacancy states are involved. In the transitions considered, a two-K-shell vacancy state is involved, which may imply larger uncertainties of the transition energies.

The natural widths of the KK-KLL hypersatellite transitions were calculated as a sum of initial-state width and final-state widths of Bhalla *et al.* [14]. The width of the initial state has been calculated using nonradiative transition probabilities from this work and the fluorescence yield of Bhalla *et al.* [14].

The total double K-shell ionization cross section was calculated as a function of electron impact energy in the classical and quantum-mechanical binary encounter approximation (BEA) [15], including the momentum transfer to the nucleus [16]. Hartree-Fock atomic wave functions were used [17].

III. EXPERIMENTAL METHOD

The measurements were performed by a gas-phase electron spectrometer. It consists of a 30° parallel plate electrostatic analyzer, an electron gun, an effusive gas beam formed by a narrow multicapillary array, and a Faraday cup. A three-element rectangular tube lens formed an image of the target region on the entrance slit of the analyzer. The analyzer was oriented at 90° with respect to the electron beam direction. Such a geometry was chosen to achieve optimal transmission for the electrons emitted from a cylindrical interaction region, formed by the intersection of the electron beam and the effusive gas target. The electrons, which passed the exit slit of the analyzer, were detected by a channel electron multiplier. A background signal of electrons scattered from the analyzer slits was strongly suppressed by applying a high negative potential to the channeltron entrance. During an energy scan, the potentials of the channeltron front and back

end were both varied according to the analyzer transmission energy in order to keep the detection efficiency constant.

The data-acquisition software was designed to allow consecutive scans over different energy regions. The system controls simultaneously up to eight power supplies. Their output voltages could either be set constant or driven as a function of the transmission energy. One of the eight voltages is chosen to define and control the transmission energy.

A constant relative resolution mode without deceleration was used to measure the spectra. In this way, a rather moderate energy resolution was chosen to favor a higher transmission necessary to measure very weak spectral structures. The analyzer plate with the entrance and exit slits was kept at ground potential. The transmission energy was defined by changing the potential of the second analyzer plate. The potential on the entrance lens was varied as a function of the transmission energy in order to keep the image of the interaction region at the entrance slit. The resulting change of the analyzer acceptance angle was neglible. The potential required on the entrance lens was obtained by numerical simulation [18]. To determine the transmission function, the measured diagram Auger lines $KL_1L_1\,^1S$ at 748.1 ± 0.1 eV, $KL_1L_{23}\,^1P$ at 771.6 ± 0.1 eV, and $KL_{23}L_{23}\,^1D$ at 804.3 ± 0.1 eV were fitted with the Voigt profiles [19]. The intensities obtained for the $KL_1L_1\,^1S$ and $KL_1L_{23}\,^1P$ lines were 0.093 ± 0.01 and 0.276 ± 0.023 of the strongest $KL_{23}L_{23}\,^1D$ line, respectively. These ratios agreed within experimental error with the results of Krause *et al.* [6] and of Albiez *et al.* [20]. This showed that the transmission of the spectrometer remained fairly constant over the measured energy regions and allowed us to normalize the observed transition in the hypersatellite energy region to the intensity of the $KL_{23}L_{23}\,^1D$ diagram line. The relative resolution (FWHM) of the fitted spectra was 1.9×10^{-3}.

The average target pressure was 50 times higher than the average pressure in the measuring chamber, which was up to 7×10^{-5} mbar. Typical electron currents were about 10 μA and the beam diameter was kept below 1 mm. The measured current of scattered charged particles hitting the gas nozzle was measured and kept well below 0.3 nA in order to suppress background counts.

The measurement cycles each consisted of a scan through the Ne KLL diagram lines between 740 eV and 820 eV, used for normalization and transmission evaluation, followed by a scan of the energy region of the predicted hyperstellite transitions. In order to reach the detection limit in the search for transitions, the hypersatellite scanning region was kept as narrow as reasonable and the accumulation time per point in this region was 20 times that in the diagram region. The yields in the separate cycles were summed together, which resulted in measuring times ranging from 3000 sec to 8000 sec per measuring point in the hypersatellite region. The resulting spectra consisted of both the diagram Auger KLL energy region, which served for normalization, and the hypersatellite region. Figure 1 shows the spectrum obtained at 5 keV electron impact energy.

Similar measurements were also performed for the energy region between 828 eV and 851 eV in an attempt to detect the KK-$KL_1L_{23}\,^2P^{(+)}$ decay channel. The attempt failed due to strong background processes in this energy region, consisting of the Lorentzian tail of the $KL_{23}L_{23}\,^1D$ diagram line and satellite transitions from the initial-state configuration $1s^12p^53p^1$ to the $2p^4\,^1S$ and $2p^4\,^1D$ [6] final states. These transitions occurred with similar intensities at energies below and significantly above threshold for the double K-shell ionization in neon, which indicates that they belong to the KLL satellite transitions.

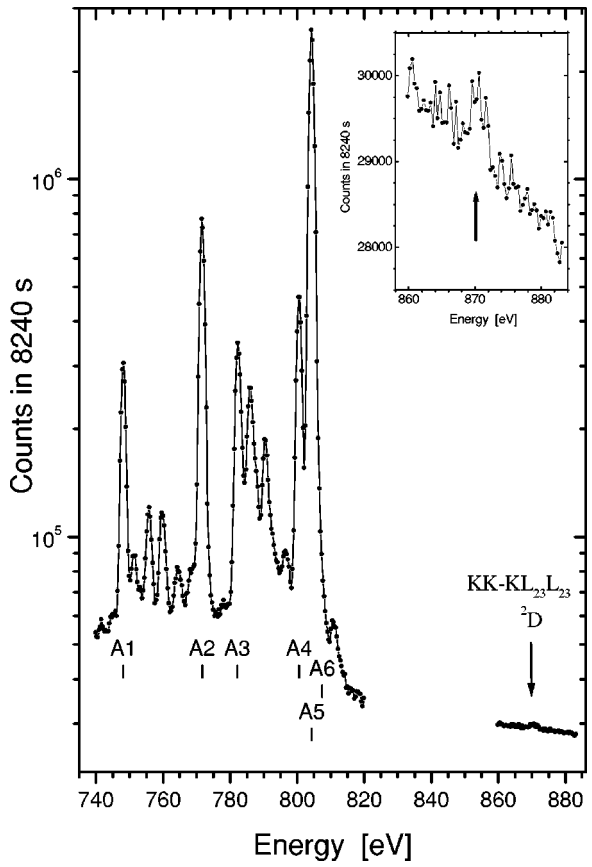

FIG. 1. Measured Auger spectrum of neon at 5 keV electron impact energy: Comparison of the signal intensity from the diagram KLL energy region between 740 eV and 820 eV and the hypersatellite energy region between 860 and 884 eV. To enable a presentation of both energy regions on the same plot, the yield in the diagram energy region was multiplied by 20. The markers $A1$–$A6$ [6] indicate energies of the diagram Auger KLL transitions $2s^o2p^6\,^1S$, $2s^12p^5\,^1P$, $2s^12p^5\,^3P$, $2p^4\,^1S$, $2p^4\,^1D$, and $2p^4\,^3P$, respectively.

IV. RESULTS

The spectra measured at 2 keV, 2.7 keV, 3.7 keV, and 5.5 keV impact energy are plotted in Fig. 2. A detection limit of three standard deviations of the background was assumed near the weak hypersatellite peak. According to this criterion, the detection limit for the peak at 870.5 ± 0.3 eV was achieved for impact energies above 3 keV. With reference to the calculations presented in Sec. II, this peak was ascribed to the KK-$KL_{23}L_{23}\,^2D$ Auger hypersatellite decay channel of the $1s^{o\,1}S$ state. The intensities of the observed ^2D peak were normalized to those of the $KL_{23}L_{23}\,^1D$ diagram line.

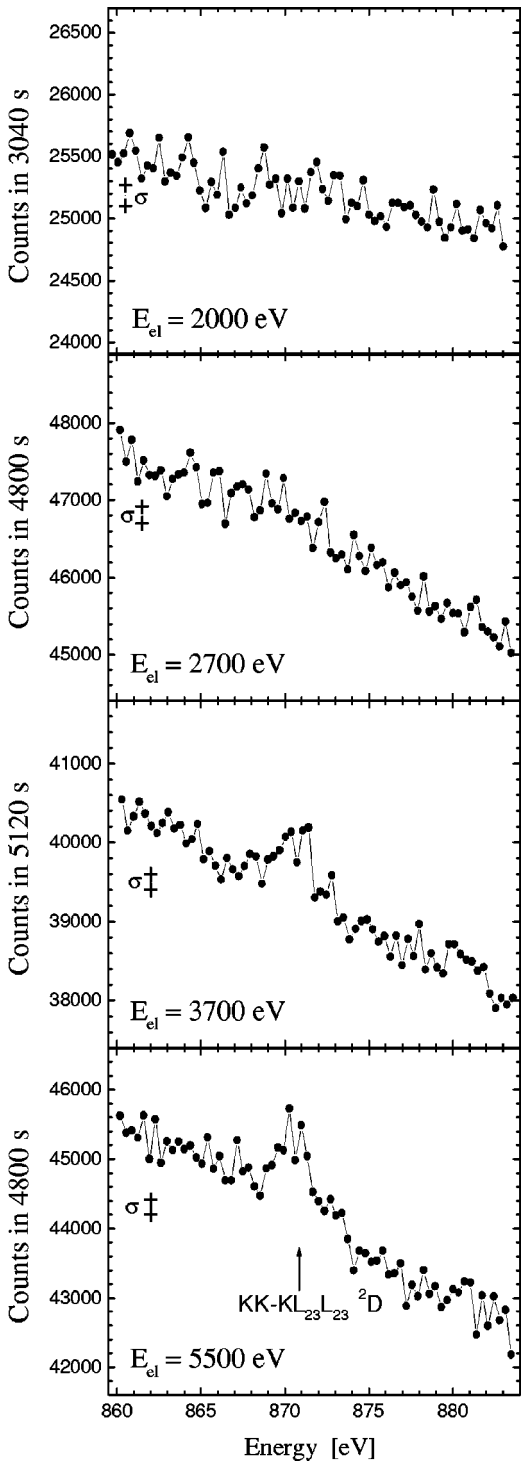

FIG. 2. Auger spectra of neon in the energy region between 860 eV and 884 eV measured at electron impact energies of 2, 2.7, 3.7, and 5.5 keV. The two crosses indicate one standard deviation of the background at 870.5 eV. The experimental resolution at 870 eV was 1.7 eV.

The respective intensity ratios $I(^2D)/I(^1D)$ are shown in Fig. 3.

The ratio of the cross section for the formation of the Ne^{2+} $1s^o\,^1S$ state with two *K*-shell vacancies to the cross section for formation of the Ne^+ $1s^{1\,2}S$ state with a single

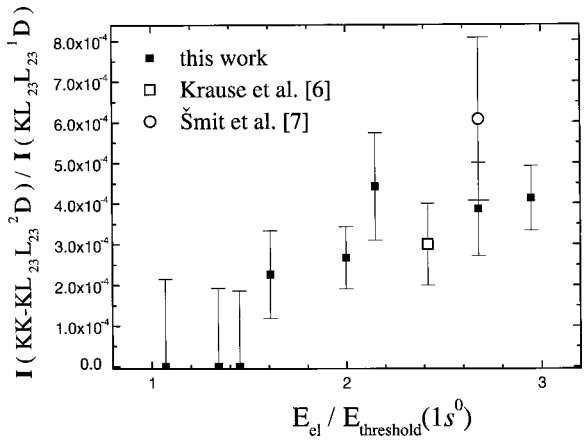

FIG. 3. The intensity ratio of the KK-$KL_{23}L_{23}{}^2D$ and $KL_{23}L_{23}{}^1D$ Auger transitions as a function of electron impact energy at 90° scattering angle. The energy unit equals 1863 eV, the double ionization energy of the neon *K* shell.

K-shell vacancy is given by

$$\frac{\sigma(1s^o,{}^1S)}{\sigma(1s^1,{}^2S)}=\frac{I(^2D)}{I(^1D)}\,\frac{\mathcal{B}(^1D)}{\mathcal{B}(^2D)}\,\frac{1-\omega(1s^{-1\,2}S)}{1-\omega(1s^{-2\,1}S)}. \tag{3}$$

Here, I denotes the intensity and ω the fluorescence yield of the respective transition. If $T_{i\to f}$ represents a transition probability from the initial state i to final state f, then the branching ratio of the diagram $KL_{23}L_{23}{}^1D$ Auger transition from the Ne^{1+} $1s^{1\,2}S$ initial state is given by

$$\mathcal{B}(^1D)=\frac{T_{i\to f}(i=1s^{1\,2}S;\,f=2p^{4\,1}D)}{\sum_f T_{i\to f}(i=1s^{1\,2}S;\,f=\{2p^4,2s^12p^5,2s^0\})}. \tag{4}$$

In our calculation we used for $\mathcal{B}(^1D)$ an experimental value of 0.61 with a 2% relative uncertainty [6,20].

The branching ratio for the hypersatellite transition KK-$KL_{23}L_{23}{}^2D$ from the initial state Ne^{2+} $1s^o\,^1S$,

$$\mathcal{B}(^2D)=\frac{T_{i\to f}(i=1s^{0\,1}S;f=1s^12p^{4\,2}D)}{\sum_f T_{i\to f}(i=1s^{0\,1}S;f=\{1s^12p^4,1s^12s^12p^5,1s^12s^0\})} \tag{5}$$

was estimated from our calculations (Table I) to be 0.49 with a relative uncertainty of 15%. The ratio (3) is not sensitive to the slightly different fluorescence yields of the $1s^{-2\,1}S$ and $1s^{-1\,2}S$ states [8,14].

The absolute cross sections for production of the Ne^{2+} $1s^o\,^1S$ state by electron impact were determined from Eq. (3) using the average experimental values of $\sigma_{K,\mathrm{tot}}$ [21]. As the initial states $1s^{-1\,2}S$ and $1s^o\,^1S$ are spherically symmetric, the angular distribution of the KLL Auger as well as of the hypersatellite KK-KLL electrons is isotropic [22]. The total *K*-shell ionization cross section also includes processes in

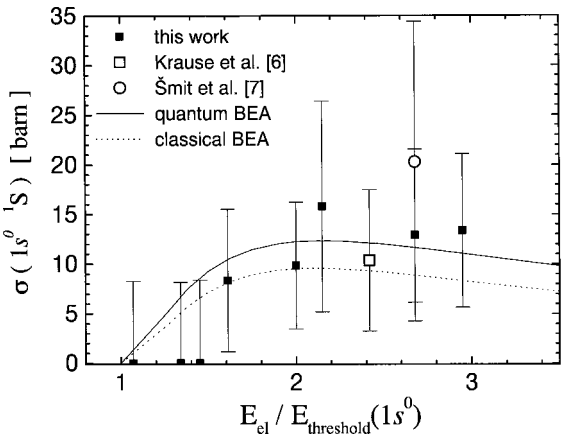

FIG. 4. The absolute cross section for production of the hollow Ne^{2+} $1s^o\,^1S$ state. The energy unit as in Fig. 3. Full line: quantum binary encounter approximation, dotted line: classical binary encounter approximation

which additional *L*-shell electrons are excited or ionized. To evaluate this contribution to the total *K*-shell ionization cross section $\sigma_{K,\mathrm{tot}}$, independent measurements were performed in the energy region of the strongest satellite transitions, called also *D* satellites, $1s^12p^5(^3P)$-$2p^3(^2P)$, $1s^12p^5(^3P)$-$2p^3(^2D)$, $1s^12p^5(^1P)$-$2p^3(^2P)$, and $1s^12p^5(^1P)$-$2p^3(^2D)$. As a result, the summed satellite intensity relative to the diagram lines was found constant with a systematic error of 10% for impact energies between 2 keV and 6 keV. This is also confirmed in the work of Albiez *et al.* [20] by a comparison of the diagram and *D*-satellite intensities at 4.5 keV and 40 keV. We assumed a similar behavior of the cross section also for other satellite states. From the results of Krause *et al.* [6] obtained at 4.5 keV, we conclude for the applied energies,

$$\sigma(1s^1,\,^2S) = 0{,}77(1\pm 0.1)\,\sigma_{K,\mathrm{tot}}. \tag{6}$$

The resulting absolute cross sections, $\sigma(1s^0,\,^1S)$ are plotted in Fig. 4. The rather large errors are introduced by error propagation from the uncertainties in the branching ratios $\mathcal{B}(^1D)$ and $\mathcal{B}(^2D)$, and from the uncertainties in the reference values for the single *K*-shell ionization cross section, $\sigma_{K,\mathrm{tot}}$.

The results of the binary encounter approximation (BEA) are compared to the experimental values in Fig. 4. For the derivation of the Ne^{2+} $1s^o\,^1S$ production cross sections $\sigma(1s^o,\,^1S)$ from the values of the total double *K*-shell ionization cross section σ_{KK}, the shakeoff process was taken into account by $\sigma(1s^o,\,^1S) = 0.54\ \sigma_{KK}$ [7]. Both BEA models agree well with the derived values, except in the region immediately above threshold, where the experimental values seem to be systematically lower than theoretical ones.

V. CONCLUSION

Electron impact spectroscopy in neon allied with theoretical calculations has enabled us to observe and identify the Ne KK-$KL_{23}L_{23}{}^2D$ Auger hypersatellite corresponding to the transition from the initial Ne^{2+} $1s^o\,^1S$ state to the final Ne^{3+} $1s^12p^4\,^2D$ state. This is the strongest decay channel of the hollow Ne^{2+} $1s^o\,^1S$ state. Its production cross section as a function of the electron impact energy was determined.

The measurements of the hypersatellite intensities with respect to the intense $KL_{23}L_{23}{}^1D$ diagram line allowed the cross section for electron impact formation of the Ne^{2+} $1s^o\,^1S$ state to be determined in the energy range up to three times the double *K*-shell ionization threshold (1863 eV). Away from the threshold, a good agreement exists between the derived experimental cross sections and those calculated using the binary encounter approximation. A maximum value for the cross section of 16 ± 10 barn was obtained at the impact energy of 4 keV. The detection of a process with such a low cross section requires an extremely stable setup with good detection efficiency.

ACKNOWLEDGMENTS

This work was done as part of Project No. J1-8876 of the Slovenian Ministry of Science and Technology. P.P. and M.Ž. gratefully acknowledge financial support by the Ministry, and I.Č. is grateful for financial support provided by the J. Stefan Institute.

[1] J.P. Briand, L. Billy, P. Charles, E. Essabas, P. Briand, R. Geller, J.P. Desclaux, S. Bliman, and C. Ristori, Phys. Rev. Lett. **65**, 159 (1990).
[2] J. Ahopelto, E. Rantavuori, and O. Keski-Rahkonen, Phys. Scr. **20**, 71 (1979).
[3] J. Auerhammer, H. Genz, G. Kilgus, A. Kumar, and A. Richter, Phys. Lett. A **35**, 4505 (1987).
[4] V. Cindro, M. Budnar, M. Kregar, V. Ramšak, and Ž. Šmit, J. Phys. B **22**, 2161 (1989).
[5] C.W. Woods, R.L. Kauffman, K.A. Jamison, N. Stolterfoht, and P. Richard, Phys. Rev. A **12**, 1393 (1975).
[6] M.O. Krause, T.A. Carlson, and W.E. Moddeman, J. Phys. (Paris), Colloq. **32**, C4-139 (1971).
[7] Ž. Šmit, M. Žitnik, L. Avaldi, R. Camilloni, E. Fainelli, A. Mühleisen, and G. Stefani, Phys. Rev. A **49**, 1480 (1994).
[8] M.H. Chen, Phys. Rev. A **44**, 239 (1991).
[9] J. Lahtinen and O. Keski-Rahkonen, Phys. Scr. **27**, 334 (1983).
[10] E. Mikkola, O. Keski-Rahkonen, and R. Kuoppala, Phys. Scr. **19**, 29 (1979).
[11] K.G. Dyall, I.P. Grant, C.T. Johnson, F.A. Parpia, and E.P. Plummer, Comput. Phys. Commun. **55**, 425 (1989).
[12] W.F. Perger, Z. Halabuka, and D. Trautmann, Comput. Phys. Commun. **76**, 250 (1993).
[13] A. Mäntykenttä, thesis, University of Oulu, Finland (1993).
[14] C.P. Bhalla, N.O. Folland, and M.A. Hein, Phys. Rev. A **8**, 649 (1973).
[15] M. Gryzinski, Phys. Rev. **138**, A305 (1965).
[16] L. Vriens, Proc. Phys. Soc. London **98**, 13 (1966).
[17] C. Froese Fischer, Comput. Phys. Commun. **43**, 355 (1987).
[18] F. H. Read and N. Bowring, CPO-3D, Charged Particle Optics

Program, Department of Physics and Astronomy, University of Manchester, UK. (see also http://cpo.ph.man.ac.uk)

[19] J. Végh, in *Proceedings of the Sixth European Conference on Applications of Surface and Interface Analysis, Montreaux, 1995*, edited by H. J. Mathieu, B Reihl, and D. Briggs (Wiley, Chicester, 1996), pp. 679–682.

[20] A. Albiez, M. Thoma, W. Weber, and W. Mehlhorn, Z. Phys. D: At., Md. Clusters **16**, 97 (1990).

[21] X. Long, M. Liu, F. Ho, and X. Peng, At. Data Nucl. Data Tables **45**, 353 (1990).

[22] N.M. Kabachnik and I.P. Sazhina, J. Phys. B **17**, 1335 (1984).